Electron transfer plus double ionization in slow He^{2+} + Ar collisions

Y. Gao,[1] M. Schulz,[2] D. L. Guo,[1] S. F. Zhang,[1,3,*] X. L. Zhu,[1] R. T. Zhang,[1] W. T. Feng,[1] D. M. Zhao,[1] and X. Ma[1,3,†]

[1]*Institute of Modern Physics, Chinese Academy of Sciences, Lanzhou 730000, China*

[2]*Department of Physics and LAMOR, Missouri University of Science & Technology, Rolla, Missouri 65409, USA*

[3]*School of Nuclear Science and Technology, University of Chinese Academy of Sciences, Beijing 100049, China*

(Received 20 April 2018; revised manuscript received 3 October 2018; published 26 December 2018)

We performed a kinematically complete experiment on double ionization accompanied by single capture in 30 keV/amu He^{2+} + Ar collisions. The data were systematically analyzed using three different techniques, namely, fully differential cross sections as a function of the electron emission angle of each electron, the correlation function, and four-particle Dalitz plots. The data can to a large extent be explained within the independent electron model. However, the correlation function reveals small but significant effects from correlations in the initial target state. These correlations strongly depend on the interaction between the nuclei of the collision partners. Furthermore, a surprisingly strong correlation between the electron momenta with the momentum transfer, reported earlier, was confirmed.

DOI: 10.1103/PhysRevA.98.062711

I. INTRODUCTION

One-electron processes in ion-atom collisions, i.e., electron capture, excitation, and ionization, have been studied extensively over the last several decades (for reviews see, e.g., [1–4]). Such studies are important in order to test the theoretical description of the few-body dynamics in systems containing a few charged particles [5,6]. Kinematically complete experiments (for reviews see, e.g., [4,7,8]), from which fully differential cross sections (FDCSs) can be extracted, offer a particularly sensitive tool to test theoretical models. The measurement of FDCSs requires one to experimentally determine the momentum vectors of all unbound collision fragments. On the other hand, not all momentum components are independent of each other due to the kinematic conservation laws. As a result, for a process involving n collision fragments the degree of differentiality of the FDCS is not given by $3n$, but rather by $3n-4$. For capture and excitation $n=2$ so that already the cross-section differential in projectile solid angle (which is a double differential) represents a FDCS. But for the three-body scattering process of ionization FDCSs are already fivefold differential. For electron impact, FDCSs for ionization have been measured already for several decades [9,10], but due to the much larger projectile mass such experiments are much more challenging for ion impact and became feasible only at the beginning of the millennium [6].

Due to this increased complexity in ionization compared to capture and excitation one might expect that the FDCSs are much richer in structure. Surprisingly, over a very broad range of kinematic conditions the FDCSs for light targets exhibit a fairly simple pattern which qualitatively does not vary much for different collision systems (e.g., [4,6,11–15]). In fact, these features can qualitatively be amazingly well reproduced by first-order calculations, which completely ignore the nucleus-nucleus (NN) interaction, although quantitatively higher-order contributions usually play an important role. Only for very slow projectiles [16] and for very large perturbation parameters (projectile charge-to-speed ratio η) [17] is a clear departure from this simple pattern observed. Furthermore, for heavier targets the nodal structure of the initial-state wave function can lead to additional features in the FDCSs [18].

For heavier targets there is a non-negligible probability that ionization is accompanied by other transitions such as capture of an additional electron from the target to the projectile or target excitation. Compared to single ionization, such processes can provide more sensitive information about the collisions dynamics. For instance, especially at large projectile energies electron-electron correlations can play an important role [19]. At small projectile energies it was demonstrated that in transfer ionization in He^{2+} on Ar collisions, mechanisms contributing to the electron emission include direct transfer ionization (i.e., the projectile captures one electron and ejects the second in two independent interactions), double-electron capture with autoionization in the projectile, and single-electron capture from an inner-shell target shell with autoionization of the target [20]. A more recent study also showed that in direct transfer ionization, the emitted electron spectra can be explained by a two-step model considering the initial electron velocity and rescattering of the binary encounter electron in the recoil potential [21].

For double ionization the measurement of FDCS becomes significantly more challenging for three reasons: (a) the degree of differentiality is increased to 8, (b) the momentum of one more collision fragment needs to be measured directly, and (c) the cross sections are usually smaller by orders of magnitude. As a result, so far only one data set on sevenfold-differential cross sections was reported [22], but measured FDCSs are not available. A kinematically complete

*zhangshf@impcas.ac.cn
†x.ma@impcas.ac.cn

experiment was also performed for triple ionization, but only double differential cross sections were reported [23].

Theoretically, double ionization by ion impact has been studied extensively [24–28]. However, the lack of measured FDCSs for multiple-ionization processes represents a major limitation in sensitively testing theoretical descriptions of the few-body dynamics. Nevertheless, several data analysis techniques, based on less differential cross sections, were developed which resulted in significant new qualitative insight into the collision dynamics of multielectron processes [29–33]. For example, the so-called correlation function (CF) proved, in spite of being based on single differential cross sections, to very sensitively reveal electron-electron correlation effects in double ionization [29]. In this method, certain spectra (for example, as a function of the momentum difference between the two ejected electrons) are generated for two electrons ejected in the same collision (and which are therefore usually affected by correlation effects) and for two electrons ejected in two subsequent double-ionization events (and which are therefore guaranteed independent of each other). Any departure of the ratio between these two spectra from 1 is a direct measure of electron-electron correlations.

Another data analysis technique that was recently developed is based on four-particle Dalitz (4-D) plots [31–33]. Originally developed to analyze three-body decays in particle physics [34], it was later applied to study atomic fragmentation processes [23,35] and was more recently extended to four-body processes. Here, the quantities that are plotted, the Dalitz coordinates, are the relative squared momentum changes of the four collision fragments $\epsilon_i = (\Delta p_i)^2/\Sigma(\Delta p_j)^2$. All four Dalitz coordinates are simultaneously presented in a single plot which is based on a tetrahedral coordinate system. Since 4-D plots only represent triple-differential cross sections (due to the boundary condition $\Sigma\epsilon_i = 1$) they are not nearly as sensitive as FDCSs to test theoretical calculations quantitatively. However, they offer two important advantages: (a) the interactions between any pair of collision fragments can be visualized in a single plot and (b) the total content of a 4-D plot represents the total cross section. This combination of detail (the cross sections are triple differential and all interactions are visible simultaneously) and comprehensiveness (the integral represents the total cross section) makes 4-D plots a very powerful tool to study the quantitative mechanisms that are mostly responsible for the process under investigation. For example, a new higher-order double-ionization mechanism could be identified in fast p + He collisions, where double ionization was thought to be dominated by first-order processes [33]. In FDCSs these mechanisms are very difficult to distinguish and, since they are plotted only for very specific kinematic conditions, their relative importance in the total cross section is difficult to evaluate.

In earlier studies on the channel of single ionization plus one electron capture in 30 keV/amu He^{2+} + Ar collisions, features of autoionization from the doubly excited recoil (projectile) after one electron captured from the inner shell of the target (two electrons captured to the projectile) can be clearly identified from the electron spectrum which is a footprint of strong electron-electron correlation [20]. However, in double ionization accompanied by electron capture to the projectile in the same collision system [36], we found that electron-electron correlations do not play an important role. Furthermore, the direction of the individual ejected electron momenta were found to be surprisingly correlated with the direction of the momentum transfer from the projectile to the target atom. In this article we present a systematic study of this process for the same collision system employing a variety of analysis techniques. First, we extend the analysis of the FDCS to a much broader range of kinematic conditions in order to determine whether the correlation between the electron momenta and momentum transfer is a general feature or merely characteristic of specific kinematic regimes. Second, we took advantage of the high sensitivity of the CF to electron-electron correlation effects to determine whether it can reveal such effects in situations where they are too weak to be observable in FDCSs. Furthermore, we wanted to test whether the universality of the CF, found earlier for pure double ionization by fast ion impact [29], extends to different processes and kinematic regimes from those studies in [29]. Finally, 4-D plots were employed to study the relative importance of interactions between pairs of particles, especially the NN interaction, in the few-body dynamics.

II. EXPERIMENT

In this experiment two ejected electrons, Ar^{3+} recoil ions, and scattered He^+ projectiles were measured in quadruple coincidence for 30 keV/amu He^{2+}+ Ar collisions. The perturbation parameter η for this collision system is 1.83. The experiment was performed at the Institute of Modern Physics, Lanzhou. The electrons and the recoil ions were momentum analyzed using a reaction microscope, which was described in detail in [20]. The He^{2+} ions produced in an electron cyclotron resonance ion source were extracted, charge analyzed, and then accelerated to the desired energy. The well-collimated ion beam entered the collision chamber and crossed vertically with a supersonic Ar gas jet in the center of the reaction microscope spectrometer. After the reaction, the projectiles with different charge states were analyzed by an electrostatic deflector downstream from the collision center, and directed to a position sensitive detector. The primary beam was collected by a Faraday cup.

The recoil ions and the electrons produced in the collision region were extracted by an electric field of 1.77 V/cm perpendicular to both the projectile and the target beam directions. The target fragments were guided to two position-sensitive detectors located at the two ends of the reaction microscope. The detectors were multihit capable so that both ejected electrons could be detected simultaneously for the same double ionization plus single capture (DISC) event. The multihit dead time was determined to be less than 30 ns. In order to optimize the resolution in the time of flight of the recoil ions from the collision region to the detector, the length ratio of the accelerating region to the drifting region of the reaction microscope was designed to be 1:2, which meets the time-focusing condition [37]. The time of flight of the fragments can be determined experimentally. Making use of their flight time and position information,

the three-dimensional momenta of the fragments can be calculated [7,8].

III. DATA ANALYSIS

From the momentum components of the collision fragments we obtained FDCS $= d^8\sigma/d^3\mathbf{p}_1 d^3\mathbf{p}_2 d^2\mathbf{q}_{tr}$. Here $\mathbf{q}_{tr}$ is the two-dimensional part of the transverse momentum transferred to the target which is perpendicular to the collision velocity. $\mathbf{p}_1$ and $\mathbf{p}_2$ are the three-momenta of the emitted electrons from the target. Furthermore, $d^3\mathbf{p}_1 = p_1^2 \sin\theta_1 dp_1 d\theta_1 d\phi_1$ and $d^3\mathbf{p}_2 = p_2^2 \sin\theta_2 dp_2 d\theta_2 d\phi_2$, where θ_1 and θ_2 are the polar angles defined by the electron momentum vectors with respect to the projectile direction, and ϕ_1 and ϕ_2 are their corresponding azimuthal angles. Only DISC events were selected in which both electrons were ejected into the scattering plane spanned by the initial projectile momentum and the momentum transfer vector $\mathbf{q}$. The scattering plane was selected because one motivation for this work was to further investigate the correlation between the electron momenta and $\mathbf{q}$ which we reported previously [36]. Furthermore, conditions were set on each electron energy (i.e., p_1 and p_2) and on the transverse component of the momentum transfer $\mathbf{q}_{tr}$. The latter condition, along with the selection of the scattering plane, defines the projectile solid angle element. The selected events are then plotted in two-dimensional plots as a function of θ_1 and θ_2, where the directions of $\mathbf{q}_{tr}$ and $-\mathbf{q}_{tr}$ define $\theta = 90^\circ$ and -90°, respectively.

Four-particle Dalitz plots were generated following the method reported in [31,32]. The quantities that are analyzed in a 4-D plot are the relative squared momentum changes of all particles in the collision: $\epsilon_i = (\Delta p_i)^2/\Sigma(\Delta p_j)^2$. In the case of the electrons and the recoil ions these momentum changes are identical to their final momenta. These Dalitz coordinates are plotted in a tetrahedral coordinate system, where each tetrahedron plane represents one particle. For a given data point a set of the four ϵ_j is given by the distances of that data point to the four tetrahedron planes. A 4-D plot can be generated using a standard Cartesian coordinate system using the following transformations:

$$\begin{aligned} x &= \epsilon_1, \\ y &= (1/\sqrt{8})(3\epsilon_2 + \epsilon_1), \\ z &= \sqrt{3/2}(\epsilon_3 + 0.5\epsilon_2 + 0.5\epsilon_1). \end{aligned} \tag{1}$$

Note that ϵ_4 is not needed in these transformations because due to the boundary condition $\Sigma\epsilon_j = 1$ only three ϵ_j are independent of each other. Data can only occur in the interior of the tetrahedron. Furthermore, the areas close to the corners, where three planes intersect, are kinematically forbidden. In these regions, momentum and energy cannot be conserved simultaneously. Right at a corner, for example, the momentum changes of the particles represented by the intersecting planes are zero and the momentum change of the fourth particle is very large (maximum distance to the fourth plane). Since $\mathbf{q} = \mathbf{p}_{rec} + \mathbf{p}_1 + \mathbf{p}_2$ the momentum changes of all particles have to be zero if they are zero for three particles.

Finally, the correlation function CF was obtained following the method described in [29]. As a first step, the magnitude of the momentum difference vector $\Delta p = |\mathbf{p}_1 - \mathbf{p}_2|$ was analyzed for two cases. In both cases only DISC events were selected by requiring true fourfold coincidences between both electrons, the recoil ions, and the charge-exchanged projectiles. One spectrum was generated for two electrons ejected in the same DISC event, which in the following we refer to as the correlated spectrum I_{cor}. The second spectrum, which we call the uncorrelated spectrum I_{unc}, was generated by randomly picking one of the two ejected electrons from the nth DISC event and one electron from the $(n+1)$th DISC event and Δp was calculated for these two completely independent electrons (event mixing). The CF is then given by $I_{cor}/I_{unc} - 1 = R - 1$. Positive values of the CF signify a correlation, i.e., the corresponding Δp are enhanced compared to independent events, and negative values signify an anticorrelation, i.e., the corresponding Δp are suppressed.

IV. RESULTS AND DISCUSSION

A. Fully differential cross sections

In Fig. 1 we show FDCSs for electrons with energies of $E_1 = E_2 = 10 \pm 5$ eV ejected into the scattering plane and for transverse momentum transfers of $q_{tr} = 3 \pm 1$ a.u. (left-hand panel), 5 ± 1 a.u. (center panel), and 8 ± 2 a.u. (right-hand panel). Equal energies of both ejected electrons were selected in order to maximize the phase-space overlap between them so that any electron-electron correlation effects, if present, would be enhanced compared to unequal energies. However, this restriction also leads to minima along the diagonal line for which $\theta_{el1} = \theta_{el2}$ where two electrons reach the detector within the multihit dead time. The dead-time area is marked in gray in the right-hand panel of Fig. 1 for illustration (as well as in Figs. 2 and 3). In the following discussions one can see that this restriction will not compromise our conclusions. The dashed lines at positive angles indicate the direction of $\mathbf{q}$ and those at negative angles the direction of $-\mathbf{q}$. Previously, we had discussed already these FDCSs for $q_{tr} = 5 \pm 1$ a.u. [36]. By comparing the data to what is usually observed in the angular dependence of the FDCSs for single ionization, we could demonstrate that the data for DISC could to a large extent be described in terms of an independent electron model (IEM). More specifically, in single ionization three structures are often observed: (a) a maximum in the direction of $\mathbf{q}$ (binary peak), (b) a weaker maximum in the direction $-\mathbf{q}$ (recoil peak), and (c) in the case of large η a maximum near $\theta = 0^\circ$ (forward peak). The FDCSs for DISC exhibit structures which are consistent with combinations of these features usually observed for single ionization. Especially the combinations "one electron is in the binary peak and the other in the forward peak" and "one electron in the recoil peak and the other in the forward peak," to which we refer as the binary/forward and recoil/forward peaks, are quite prominent.

For $q_{tr} = 5$ a.u. the FDCSs look almost identical to those for $q_{tr} = 3$ a.u. and are thus also consistent with the IEM. Qualitatively, this also holds for $q_{tr} = 8$ a.u.; however, quantitatively, there is a significant difference from the smaller momentum transfers: the intensity of the recoil/forward peak relative to the binary/forward peak is considerably enhanced. Furthermore, an additional structure is now visible, which is

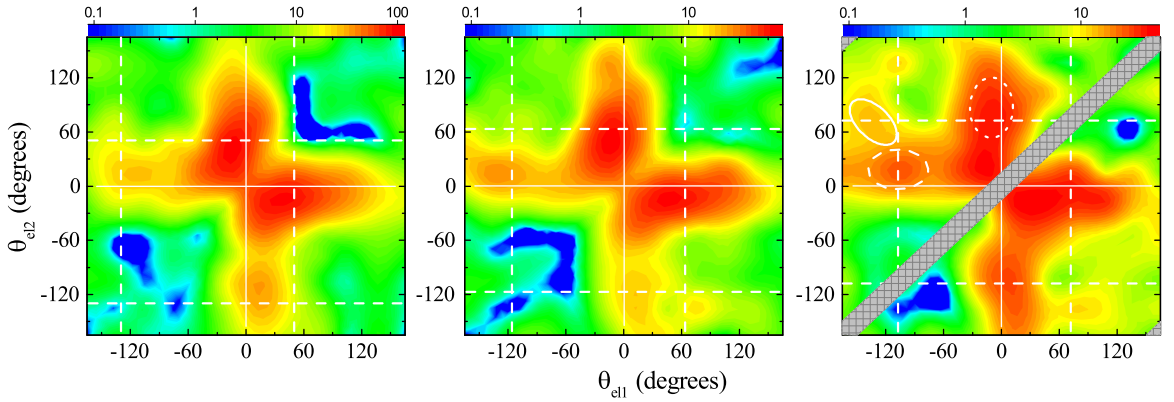

FIG. 1. Fully differential cross sections for DISC for both electrons with energies $E_1 = E_2 = 10 \pm 5$ eV ejected into the scattering plane as a function of the two polar electron ejection angles. The momentum transfer was fixed at 3 ± 1 a.u. (left-hand panel), 5 ± 1 a.u. (center panel), and 8 ± 2 a.u. (right-hand panel). The dashed lines at positive (negative) angles indicate the direction of $\mathbf{q}$ ($-\mathbf{q}$). As illustrated in the right-hand panel, the dotted, dashed, and solid circles mark the regimes of the binary/forward, the recoil/forward, and the binary/recoil peaks, respectively. The shaded area marks the minima zone due to the multihit dead time (see the text).

absent for $q_{tr} = 3$ and 5 a.u. Here, one electron is ejected in the direction of $\mathbf{q}$ and the other nearly in the direction of $-\mathbf{q}$ (binary/recoil peak). This enhanced intensity of electrons ejected in the direction of $-\mathbf{q}$ at large q has not been observed yet for single ionization, where the recoil-to-binary peak intensity ratio usually increases systematically with increasing q.

In Fig. 2 we present FDCSs for the same q_{tr} as in Fig. 1, but for electron energies $E_1 = E_2 = 20 \pm 5$ eV. The comparison with Fig. 1 suggests that the FDCS change more sensitively with the electron energies than with $\mathbf{q}$. Several differences from the FDCS for 10 eV can be seen. First, the binary/forward structures are shifted in the forward direction relative to $\mathbf{q}$, especially at large q. Such a shift is also observed in single ionization in collision systems with relatively large η. It is caused by the postcollision interaction (PCI) between the outgoing projectile and the electron(s) already lifted to the continuum by a preceding primary interaction with the projectile. PCI is known to maximize for electron energies (cusp energy) corresponding to speeds close to the projectile speed [38]. For the present collision system the cusp energy is 16.5 eV, which lies within the energy bin for which the FDCSs are presented in Fig. 2. It should be noted that the cusp peak in the electron energy spectra is very narrow, especially when electron ejection is accompanied by electron capture (e.g., [39]). Thus, cusp electron production is almost completely contained in the energy bin of 20 ± 5 eV, while it contributes very little to the energy bin 10 ± 5 eV.

The second difference from the FDCS for 10 eV is that the structures are narrower. As a result, the recoil/forward and binary/forward peaks are more separated from each other by more pronounced minima. A narrowing of the binary and recoil peaks with increasing energy is routinely found for single ionization as well (e.g., [4]). Finally, at $q_{tr} = 8$ a.u. the recoil/forward structures are considerably shifted backwards relative to $\mathbf{q}$. This observation cannot be explained by the features usually found in single ionization, where a backward shift of the recoil peak has not been reported yet. Therefore, the FDCSs for large electron energies and large $\mathbf{q}$ cannot be completely described within the IEM.

The FDCSs for $E_1 = E_2 = 5$ eV are plotted in Fig. 3. Here again, similar features as for 10 and 20 eV are observed. However, in addition the binary/recoil peaks, which for 10 eV are only seen at the largest q_{tr} and essentially absent for 20 eV, are quite prominent for all q_{tr} at 5 eV. This shows that the recoil peak increases not only with

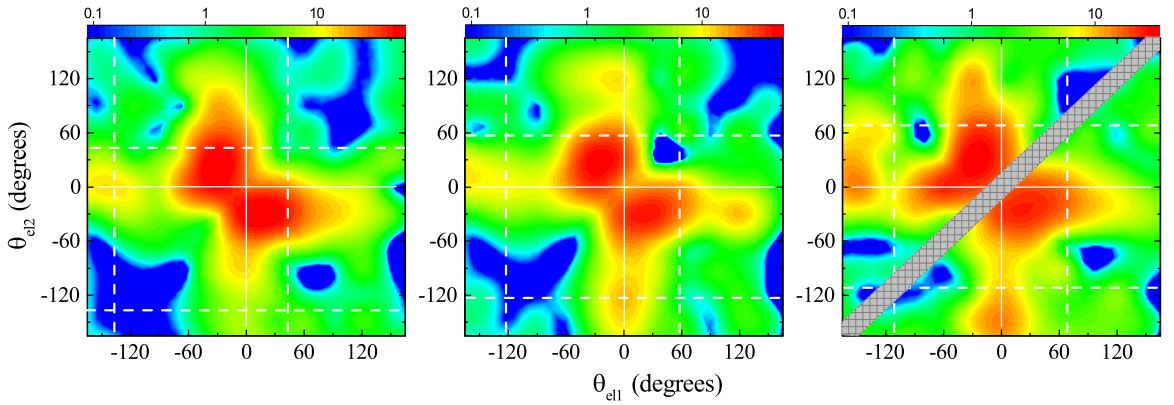

FIG. 2. Same as Fig. 1 for $E_1 = E_2 = 20 \pm 5$ eV.

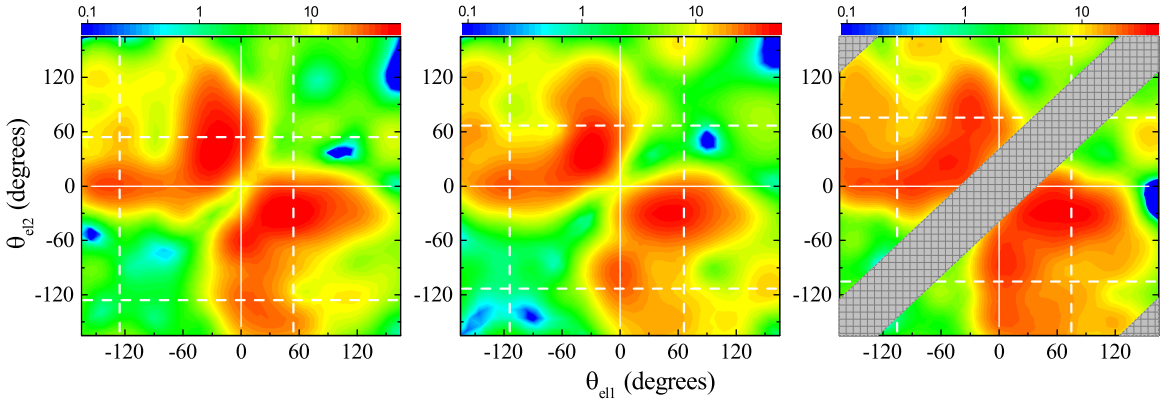

FIG. 3. Same as Fig. 1 for $E_1 = E_2 = 5 \pm 5$ eV.

increasing q_{tr}, but also with decreasing electron energy, in accordance with single ionization. An interesting observation concerns the location of the maxima involving recoil peak electrons: the recoil/forward peak occurs in the direction of $-\mathbf{q}$ (and in the forward direction for the other electron). However, for the two larger q_{tr} the binary/recoil peak is shifted backward in the recoil peak component. A closer inspection of the FDCS for 10 eV reveals a similar behavior; however, there it is not as prominent because the binary/recoil peak is much weaker than at 5 eV.

Overall, the correlation between each electron momentum and $\mathbf{q}$, initially reported for electron energies of 10 eV, is not just limited to a narrow kinematic regime. Rather, it is observed for several electron energies.

B. Four-particle Dalitz plots

In the left-hand panel of Fig. 4 a 4-D plot is shown for the longitudinal components of the momentum changes of all four collision fragments; i.e., the Dalitz coordinates are calculated as $\epsilon_{i\parallel} = (\Delta p_{i\parallel})^2 / \Sigma(\Delta p_{j\parallel})^2$. The number of counts is represented in terms of the size of the data points; the color serves to make the optical representation clearer. The front and bottom planes represent the ejected electrons, the right plane the projectile, and the back plane the recoil ion, as illustrated in the right-hand panel of Fig. 4.

A 4-D plot shows which type of interaction leads to the largest momentum exchange in the collision. For example, for data points located at one of the intersection lines between two planes, the Dalitz components for the two particles represented by the intersecting planes are zero. Therefore, here momentum exchange occurs only between the other two particles. Likewise, data points located in the center of one of the tetrahedron planes have a distance of zero to that plane, but large distances to the other three planes. Here, a relatively large momentum exchange occurs between the three particles which are not represented by the plane where the data point is located.

In the data a strong peak structure is found at the intersection line between the two planes representing the ejected electrons. Therefore, in the longitudinal direction DISC is dominated by a momentum exchange between the nuclei of the collision system. At first glance, this may appear to be surprising and indeed such a dominance of the nucleus-nucleus interaction in the longitudinal direction has never been observed for double ionization [32]. This can be understood by

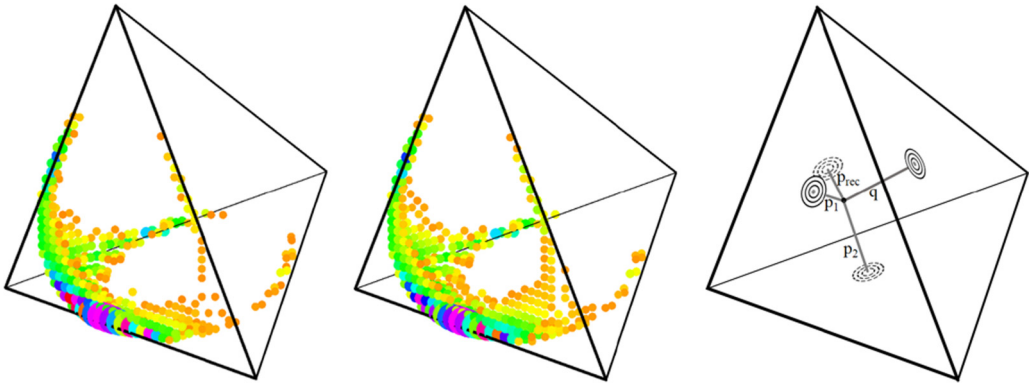

FIG. 4. Four-particle Dalitz plot for the longitudinal momentum components (for Dalitz coordinates, see text). The front and bottom planes represent the ejected electrons, the right plane the projectile, and the back plane the recoil ion. The Dalitz coordinates are given by the distance of a data point to the four planes representing the corresponding particle where angles between each of two coordinates are constant and have no physical meanings (the right-hand panel). The data in the left-hand panel were obtained for two electrons and the recoil ion produced in the same DISC event. The data in the middle panel were obtained from two electrons and the recoil ion all produced in three different DISC events (event mixing). In each case the momentum transfer was obtained from $\mathbf{q} = \mathbf{p_1} + \mathbf{p_2} + \mathbf{p_{rec}}$.

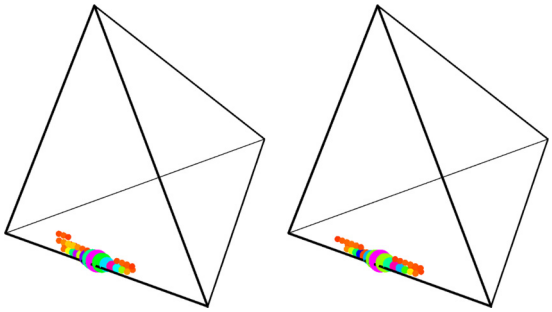

FIG. 5. Same as Fig. 4 for the transverse momentum components.

considering the relatively large negative Q value for DISC and the small projectile speed, which determine the longitudinal momentum transfer and recoil-ion momentum by [7]

$$\begin{aligned} q_\parallel &= -\Delta p_\parallel = (-Q + E_1 + E_2)/v - v/2, \\ p_{\mathrm{rec}\parallel} &= q_\parallel - p_{1\parallel} - p_{2\parallel} \\ &= (-Q + E_1 + E_2)/v - v/2 - p_{1\parallel} - p_{2\parallel}. \end{aligned} \quad (2)$$

For example, for $Q = -70$ eV, $v = 1.1$ a.u., and equal electron energies of about 13.6 eV (i.e., $p_{el\parallel} < 1$ a.u.), this yields $q_\parallel = 2.8$ a.u., which is much larger than the electron momenta. Although the corresponding recoil momentum could be as small as 0.8 a.u., in most cases it will be considerably larger than the electron momenta because on average only a certain fraction of the electron energy stems from their longitudinal motion. Furthermore, the electron momenta can be negative, which increases the recoil momentum. In contrast, for double ionization FDCSs so far were only reported for much larger projectile speeds so that there $q_\parallel$ is always relatively small.

Further maxima occur at the intersection lines between the recoil plane and one of the electron planes. These present longitudinal momentum exchange mainly between the projectile and the respective other electron. Such a configuration is only possible if one electron has a very small and the other electron a relatively large energy. According to Eqs. (2), for more symmetric energies the longitudinal recoil-ion momentum cannot become smaller than both electron momenta. The contributions near the lower left corner of the tetrahedron can be understood by similar arguments: here, momentum exchange occurs between all four particles, where the projectile transfers approximately equal fractions to the two electrons and the recoil ion. This is the configuration predicted by Eqs. (2) for similar small electron energies ejected at relatively small angles relative to the projectile beam direction.

In the left-hand panel of Fig. 5 a 4-D plot is shown for the transverse components of the momentum changes of all four collision fragments. Here, the various particles are represented by the same tetrahedron planes as in the plot for the longitudinal momentum components. This plot reveals much less structure than the one for the longitudinal components. In fact, in this spectrum we observe exclusively events in which by far the largest momentum exchange occurs between the two nuclei in the collision system. This is quite remarkable because, contrary to the longitudinal direction, significantly larger momenta of the nuclei compared to the electrons are not simply strongly favored by the kinematic conservation laws [i.e., by Eqs. (2)]. Rather, the dominance of the NN interaction provides information about the collision dynamics. More specifically, one can conclude that DISC is quite selective on small impact parameters, which was not necessarily expected for such a small projectile energy. For double ionization the NN interaction also tends to be dominant in the 4-D plots; however, there additional structures were always observed at the intersection lines representing binary momentum exchange between the projectile and one electron [32]. This suggests that the high selectivity of DISC on close collisions is mainly due to the capture step.

One might expect that electron-electron correlations are signified in a 4-D plot by a peak structure at the intersection line between the projectile and recoil planes. However, this is not the case; even for very fast collisions, where such effects are known to play an important role in double ionization, the flux in this region actually minimized. The reason is that any inelastic process in atomic scattering always requires a primary interaction between the projectile and at least one electron. For any subsequent interaction between the electrons their energies are very small compared to the projectile energy and it is thus difficult to exchange momentum comparable to or larger than in the primary interaction. Therefore, 4-D plots are not particularly well suited to study electron-electron correlation effects, unless measured plots can be compared to reliable theoretical calculations accounting for such effects or to simulations of the expected plots based on the IEM.

We have analyzed such simulated 4-D plots based on the IEM. This was accomplished by using event mixing, i.e., the same method used to generate the correlation function (see the next section), except that the momenta of two electrons and a recoil ion were mixed from three different DISC events. This procedure enforces that the ejected electrons (and the recoil ion) are completely independent of each other. The momentum transfer was then calculated from $\mathbf{q} = \mathbf{p_1} + \mathbf{p_2} + \mathbf{p_{rec}}$ so that the momentum is still conserved for each mixed event. Therefore, in the plot obtained from event mixing the data are confined to the same region within the tetrahedron as the real events. These plots are shown in the right-hand panels of Figs. 4 and 5 for the longitudinal and transverse momentum components, respectively. Just like in the case of the CF, here too the spectra obtained for event mixing represent the IEM. It is remarkable that within statistical fluctuations no difference at all to the spectra using the momenta from the same event can be discerned, either for the longitudinal or for the transverse components.

C. Correlation function

While the FDCS and the 4-D plots can to a large extent be explained in terms of the IEM they do not reveal conclusively whether electron-electron correlation effects are just weak or essentially absent. To investigate the role of such correlation effects more sensitively than it is possible with the FDCS or 4-D plots, we analyzed the data in terms of the correlation function. The CF as a function of Δp is shown in Fig. 6 as closed circles. For comparison, we also show as open squares the CF for 3.6 MeV/amu Au^{53+} + He [29]. Qualitatively, the data are somewhat similar for both collision systems. In both

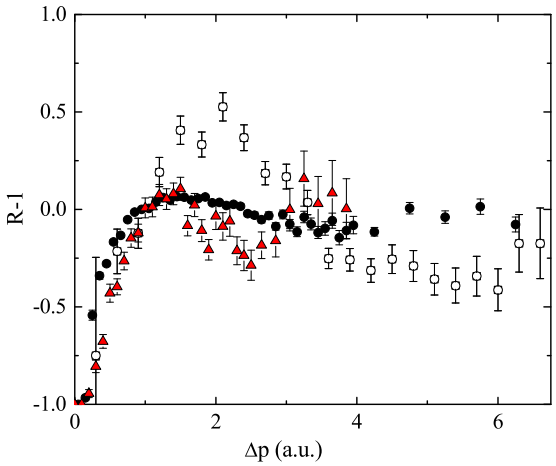

FIG. 6. Correlation function, i.e., the intensity ratio between spectra obtained for electrons emitted in the same DISC event relative to those obtained for two electrons from two different DISC events (event mixing), as a function of the magnitude of the momentum difference vector. Closed circles, present data; red triangles, present data with additional condition on the ratio of electron to recoil-ion momentum (see text); open squares, double ionization in 3.6 MeV/amu Au^{53+} + He [29].

cases a strong anticorrelation is observed at very small Δp, followed by a maximum near $\Delta p = 1.5$–2 a.u. and a (weak in the case of the DISC data) minimum near $\Delta p = 3.5$–5.5 a.u. Quantitatively, there are two differences between both data sets: the maximum and minimum are much less pronounced for He^{2+} + Ar collisions and occur at smaller Δp.

The strong anticorrelation observed for small Δp is a trivial manifestation of the fact that the ejected electrons repel each other. At the detector the electrons have departed to macroscopic distances from the nuclei of the collision system which can thus not compensate this repulsion. Therefore, the electrons cannot be at rest relative to each other. This anticorrelation should be essentially independent of the collision system and indeed in this region the CFs are practically identical for both data sets.

In [29] the CF was measured for three different collision systems with largely different η (0.1 and 4.4) and targets (He and Ne). For all three cases the CFs were remarkably similar. From this similarity the authors concluded that deviations from zero in the CF do not reflect dynamic correlation effects during the transition because such correlations are believed to sensitively depend on η. More specifically, for $\eta \ll 1$ double ionization is expected to predominantly proceed through a first-order process, in which only one electron is ejected by a direct interaction with the projectile and the second electron by an interaction with the first electron. In contrast, for $\eta \gg 1$ double ionization is mostly caused by two independent interactions of the projectile with the electrons. It was therefore concluded, and later confirmed in a follow-up paper [20], that the maximum and the minimum in the CF must be due to electron-electron correlations in the initial target state. With this interpretation one would have to conclude that the initial-state correlation among the three active electrons in DISC of Ar is significantly weaker than among the two active electrons in double ionization of He. This can partly be explained by the smaller size of the He atom compared to Ar, i.e., the on-average smaller mutual distance between the electrons.

Another factor that could be important in explaining the seemingly weaker initial-state correlation for the He^{2+} + Ar case is the involvement of the capture of one electron in addition to double ionization. The 4-D plots (Fig. 5) suggest that capture selects very small impact parameters leading to an overpowering role of the nucleus-nucleus interaction in the collision dynamics. The analysis of [29] assumed that the effects of interactions other than the electron-electron interaction "cancel" to a large extent in the CF. However, while this is probably a realistic assumption for the very fast collisions studied in [29], in which no capture selecting small impact parameters was involved, this may not be the case under the conditions realized in DISC at slow collisions leading to an extremely strong nucleus-nucleus interaction.

In order to test the effect of the nucleus-nucleus interaction we have analyzed the CF with an additional condition on the ratio between the sum momentum of both ejected electrons and the recoil momentum $R = (|\mathbf{p}_{el1} + \mathbf{p}_{el2}|)/p_{\mathrm{rec}}$. Earlier, it was demonstrated that by setting a condition on values of R significantly larger than 1 events can be selected in which the nucleus-nucleus interaction is relatively weak [40,41]. One might therefore expect that with such a condition the CF for the He^{2+} + Ar data become more similar to the CF for double ionization in fast collisions. The CF with a condition on $R > 3$ is shown as red triangles in Fig. 6. The condition on R leads to a significant alteration of the CF. The anticorrelation at $\Delta p = 0$ is more pronounced (i.e., extends to larger Δp) and the minimum is shifted to $\Delta p = 2.5$ a.u. and is also more pronounced than in the CF without a condition on R. However, this does not lead to a closer resemblance to the data for double ionization in Au^{53+} + He collisions.

These observations suggest the following:

(1) The CF is significantly affected by how strong the nucleus-nucleus interaction is relative to the other interactions involved in the collision dynamics.

(2) This means that the universality of the CF observed for a broad variety of collision systems in [29] has its limits. At this point it is not clear whether this limit is mostly set by the very small projectile speed or by the involvement of the capture of one electron in addition to double ionization studied in [29].

(3) Even at this very small projectile speed, where correlated multielectron transition mechanisms are known to be very weak, the CF still reveals remarkably pronounced signatures of correlation effects, at least if the nucleus-nucleus interaction is suppressed. This illustrates the extreme sensitivity of the CF to such effects.

V. CONCLUSIONS

We have performed a kinematically complete experiment on double ionization accompanied by capture of a third electron to the projectile. The data were systematically analyzed using techniques developed only in relatively recent years. Earlier, we had found already that FDCSs reveal a surprising correlation between the individual ejected electron momenta and the momentum transfer. At the same time, no signatures

of electron-electron correlations could be found in the FDCS and, not surprisingly, the data can be well explained within an IEM. These findings were confirmed in the present work for additional data sets under different kinematic conditions.

Furthermore, we analyzed 4-D plots. In the case of double ionization the dominant reaction mechanism could be identified by comparing experimental data to various theoretical models. In the present case, theoretical calculations are not yet available, which makes the interpretation of the data much more challenging. Nevertheless, some important information about the momentum balance between two or more particles in the collision system could be extracted from the 4-D plots. For example, the overpowering role of the nucleus-nucleus interaction (as far as momentum, but not energy exchange, is concerned) was revealed. This makes the strong correlation between each electron and the momentum transfer even more surprising.

Finally, the CF proved to be a very sensitive tool for electron-electron correlations in the initial target state. While the FDCS and 4-D plots do not reveal any signatures of such correlations at all, analyzing the CF showed small but significant effects. The CF may therefore be well suited to analyze the role of initial-state correlations also of more complex targets including molecules. However, our data also show that if the nucleus-nucleus interaction is extremely strong, as illustrated by the 4-D plots, it may significantly alter the shape of the CF. This also means that due to the NN interaction the apparent universality of the CF observed for double ionization by energetic ion impact has its limits. Therefore, studies of initial-state correlations using the CF should be performed under kinematic conditions under which the nucleus-nucleus interactions is minimized.

ACKNOWLEDGMENTS

This work is jointly supported by the National Key Research and Development Program of China under Grant No. 2017YFA0402300, and by the National Natural Science Foundation of China under Grants No. 10979007 and No. 11574327. S.F.Z. is grateful for the support from the program "One Hundred Talented People" of the Chinese Academy of Sciences. Y.G. acknowledges the support of the CAS "Light of West China" Program under Grant No. 29Y702020. M.S. is grateful for a visiting professorship from the CAS President's International Fellowship Initiative and for the hospitality of the Institute of Modern Physics. He also acknowledges support from the National Science Foundation under Grant No. PHY-1703109. We would like to thank the engineers who operated the 320 kV platform for their assistance in running the ECR ion source.

[1] J. Park, Adv. At. Mol. Phys. **19**, 67 (1983).
[2] D. c. v. Belkić, I. Mančev, and J. Hanssen, Rev. Mod. Phys. **80**, 249 (2008).
[3] N. Stolterfoht, R. D. DuBois, and R. D. Rivarola, *Electron Emission in Heavy Ion-Atom Collisions*, Springer Series on Atomic, Optical, and Plasma Physics (Springer, Berlin, 1997).
[4] M. Schulz and D. H. Madison, Int. J. Mod. Phys. A **21**, 3649 (2006).
[5] T. N. Rescigno, M. Baertschy, W. A. Isaacs, and C. W. McCurdy, Science **286**, 2474 (1999).
[6] M. Schulz, R. Moshammer, D. Fischer, H. Kollmus, D. H. Madison, S. Jones, and J. Ullrich, Nature (London) **422**, 48 (2003).
[7] J. Ullrich, R. Moshammer, A. Dorn, R. Dörner, L. P. H. Schmidt, and H. Schmidt-Böcking, Rep. Prog. Phys. **66**, 1463 (2003).
[8] R. Dörner, V. Mergel, O. Jagutzki, L. Spielberger, J. Ullrich, R. Moshammer, and H. Schmidt-Böcking, Phys. Rep. **330**, 95 (2000).
[9] H. Ehrhardt, M. Schulz, T. Tekaat, and K. Willmann, Phys. Rev. Lett. **22**, 89 (1969).
[10] H. Ehrhardt, K. Jung, G. Knoth, and P. Schlemmer, Z. Phys. D **1**, 3 (1986).
[11] D. Fischer, R. Moshammer, M. Schulz, A. B. Voitkiv, and J. Ullrich, J. Phys. B **36**, 3555 (2003).
[12] N. V. Maydanyuk, A. Hasan, M. Foster, B. Tooke, E. Nanni, D. H. Madison, and M. Schulz, Phys. Rev. Lett. **94**, 243201 (2005).
[13] A. B. Voitkiv, B. Najjari, R. Moshammer, M. Schulz, and J. Ullrich, J. Phys. B **37**, L365 (2004).
[14] M. Schulz, B. Najjari, A. B. Voitkiv, K. Schneider, X. Wang, A. C. Laforge, R. Hubele, J. Goullon, N. Ferreira, A. Kelkar, M. Grieser, R. Moshammer, J. Ullrich, and D. Fischer, Phys. Rev. A **88**, 022704 (2013).
[15] H. Gassert, O. Chuluunbaatar, M. Waitz, F. Trinter, H.-K. Kim, T. Bauer, A. Laucke, C. Müller, J. Voigtsberger, M. Weller, J. Rist, M. Pitzer, S. Zeller, T. Jahnke, L. P. H. Schmidt, J. B. Williams, S. A. Zaytsev, A. A. Bulychev, K. A. Kouzakov, H. Schmidt-Böcking, R. Dörner, Y. V. Popov, and M. S. Schöffler, Phys. Rev. Lett. **116**, 073201 (2016).
[16] L. P. H. Schmidt, M. S. Schöffler, K. E. Stiebing, H. Schmidt-Böcking, R. Dörner, F. Afaneh, and T. Weber, Phys. Rev. A **76**, 012703 (2007).
[17] M. Schulz, R. Moshammer, A. Perumal, and J. Ullrich, J. Phys. B **35**, L161 (2002).
[18] R. Hubele, A. LaForge, M. Schulz, J. Goullon, X. Wang, B. Najjari, N. Ferreira, M. Grieser, V. L. B. de Jesus, R. Moshammer, K. Schneider, A. B. Voitkiv, and D. Fischer, Phys. Rev. Lett. **110**, 133201 (2013).
[19] J. H. McGuire, *Electron Correlation Dynamics in Atomic Collisions* (Cambridge University Press, Cambridge, U.K., 1997).
[20] X. Ma, R. T. Zhang, S. F. Zhang, X. L. Zhu, W. T. Feng, D. L. Guo, B. Li, H. P. Liu, C. Y. Li, J. G. Wang, S. C. Yan, P. J. Zhang, and Q. Wang, Phys. Rev. A **83**, 052707 (2011).
[21] Y. Gao, X.-L. Zhu, S.-F. Zhang, R.-T. Zhang, W.-T. Feng, D.-L. Guo, B. Li, D.-M. Zhao, H.-B. Wang, Z.-K. Huang, S.-C. Yan, D.-B. Qian, and X.-W. Ma, Chin. Phys. Lett. **33**, 073401 (2016).
[22] D. Fischer, R. Moshammer, A. Dorn, J. R. Crespo López-Urrutia, B. Feuerstein, C. Höhr, C. D. Schröter, S. Hagmann, H. Kollmus, R. Mann, B. Bapat, and J. Ullrich, Phys. Rev. Lett. **90**, 243201 (2003).
[23] M. Schulz, R. Moshammer, W. Schmitt, H. Kollmus, R. Mann, S. Hagmann, R. E. Olson, and J. Ullrich, Phys. Rev. A **61**, 022703 (2000).

[24] M. Foster, J. Colgan, and M. S. Pindzola, J. Phys. B **41**, 111002 (2008).
[25] X. Guan and K. Bartschat, Phys. Rev. Lett. **103**, 213201 (2009).
[26] L. Gulyás, L. Sarkadi, A. Igarashi, and T. Kirchner, Phys. Rev. A **82**, 032705 (2010).
[27] S. D. López, S. Otranto, and C. R. Garibotti, Phys. Rev. A **89**, 062709 (2014).
[28] M. J. Ambrosio, D. M. Mitnik, L. U. Ancarani, G. Gasaneo, and E. L. Gaggioli, Phys. Rev. A **92**, 042704 (2015).
[29] M. Schulz, R. Moshammer, W. Schmitt, H. Kollmus, B. Feuerstein, R. Mann, S. Hagmann, and J. Ullrich, Phys. Rev. Lett. **84**, 863 (2000).
[30] M. Schulz, R. Moshammer, L. Gerchikov, S. Sheinerman, and J. Ullrich, J. Phys. B **34**, L795 (2001).
[31] M. Schulz, D. Fischer, T. Ferger, R. Moshammer, and J. Ullrich, J. Phys. B **40**, 3091 (2007).
[32] D. Fischer, M. Schulz, K. Schneider, M. F. Ciappina, T. Kirchner, A. Kelkar, S. Hagman, M. Grieser, K.-U. Kühnel, R. Moshammer, and J. Ullrich, Phys. Rev. A **80**, 062703 (2009).
[33] M. Schulz, M. F. Ciappina, T. Kirchner, D. Fischer, R. Moshammer, and J. Ullrich, Phys. Rev. A **79**, 042708 (2009).
[34] R. Dalitz, The London Edinburgh Dublin Philos. Mag. J. Sci. **44**, 1068 (1953).
[35] L. M. Wiese, O. Yenen, B. Thaden, and D. H. Jaecks, Phys. Rev. Lett. **79**, 4982 (1997).
[36] Y. Gao, S. F. Zhang, M. Schulz, X. L. Zhu, R. T. Zhang, W. T. Feng, D. L. Guo, D. M. Zhao, and X. Ma, J. Phys. B **50**, 10LT01 (2017).
[37] W. C. Wiley and I. H. McLaren, Rev. Sci. Instrum. **26**, 1150 (1955).
[38] A. Salin, J. Phys. B **2**, 631 (1969).
[39] D. Fregenal, J. Fiol, G. Bernardi, S. Suárez, P. Focke, A. D. González, A. Muthig, T. Jalowy, K. O. Groeneveld, and H. Luna, Phys. Rev. A **62**, 012703 (2000).
[40] H. Kollmus, R. Moshammer, R. E. Olson, S. Hagmann, M. Schulz, and J. Ullrich, Phys. Rev. Lett. **88**, 103202 (2002).
[41] M. Schulz, T. Ferger, D. Fischer, R. Moshammer, and J. Ullrich, Phys. Rev. A **74**, 042705 (2006).